Copyright © 2025 by The Journal of Bone and Joint Surgery, Incorporated

Experimentally Induced Femoroacetabular Impingement Results in Hip Osteoarthritis

A Novel Platform to Study Mechanisms of Hip Disease

Tomoyuki Kamenaga, MD, PhD, Kenichi Kikuchi, MD, PhD, Regis J. O'Keefe, MD, PhD, John C. Clohisy, MD, and Cecilia Pascual-Garrido, MD, PhD

Investigation performed at Washington University in St. Louis School of Medicine, St. Louis, Missouri

Background: We previously established a small animal model of femoral head-neck cam-type hip deformity by inducing physeal injury in immature rabbits. We investigated whether this induced deformity led to hip osteoarthritis (OA) within 4 months.

Methods: Six-week-old immature New Zealand White rabbits underwent surgery to induce physeal injury in the right femoral head, causing growth arrest and secondary head-neck deformity. Animals were divided into early-pre-OA (4 weeks) and late-OA (16 weeks) groups. Left hips served as (nonsurgical) controls. Radiographs were made to visualize deformities and OA progression. The Beck classification was used to assess macroscopic cartilage damage and OA on the acetabulum and femoral head. Micro-computed tomography (CT), histological scoring, and gene expression were used to evaluate OA progression. The Wilcoxon signed-rank test was used for group comparisons. Significance was set at $p < 0.05$.

Results: At 16 weeks, the injured hips showed radiographic evidence of joint space narrowing and a higher OA grade than the control hips ($p = 0.0002$). Micro-CT confirmed degenerative OA changes and a higher femoral head bone volume fraction (BV/TV) and trabecular thickness (Tb.Th) in the injured hips than in the control hips (BV/TV: $p = 0.0001$, Tb.Th: $p = 0.0007$). Macroscopically, the injured hips exhibited a greater prevalence and severity of chondral lesions at 4 weeks (83.3%, $p = 0.015$) and 16 weeks (100.0%, $p = 0.002$) post-injury compared with the control hips (0%), with worsening over time (4 versus 16 weeks: $p = 0.016$). The Osteoarthritis Research Society International (OARSI) score and synovitis score increased from 4 to 16 weeks post-injury. Compared with the control hips, the injured hips showed decreased *Col2* expression and increased *Col10* and *MMP13* expression at 16 weeks post-injury ($p = 0.062$, $p = 0.016$, $p = 0.041$, respectively), confirming catabolism and OA progression.

Conclusions: To our knowledge, we have created the first small animal model of hip OA secondary to experimentally induced head-neck deformity. In this model, the deformity resulted in hip OA at 16 weeks post-injury.

Clinical Relevance: This model can be used to test future interventional therapies and study mechanisms of femoroacetabular impingement-mediated hip OA.

Femoroacetabular impingement (FAI) is the leading cause of hip pain in young adults and is recognized to play an etiologic role in hip osteoarthritis (OA)[1,2]. Although the clinical and morphological abnormalities in hip FAI have been well characterized, the biological mechanisms underlying FAI and the progression of hip OA secondary to FAI remain unknown. Several molecular biology analyses have suggested that cartilage at the impingement region in symptomatic FAI is metabolically and catabolically active and may be a structural originator of hip OA[3-6]. Additionally, recent transcriptome analyses identified key molecules and pathways that contribute to hip OA during FAI and potential investigation targets for future interventional therapies[7].

Disclosure: This study was supported in part by NIH K08 Clinical Investigator Award 1K08AR077740-01, NIH R01 Award R01AR069605, an OREF/Goldberg Research Grant in Arthritis, an OREF Mentored Clinician Scientist Grant, and an OREF Etiology of the Hip Osteoarthritis Research Grant. The Curing Hip Disease Fund and Jackie and Randy Baker Research Funds provided partial support for the research personnel. The **Disclosure of Potential Conflicts of Interest** forms are provided with the online version of the article (http://links.lww.com/JBJS/I556).

However, the ability to translate these discoveries into clinical practice is limited without animal models that can serve as a platform to study the cellular and molecular mechanisms of disease. To date, most OA animal models have focused on knee joints. However, the lack of proven commonalities between knee and hip joints during early OA stages suggests that the mechanisms of degeneration differ between joints[8-10] and underscores the need for small animal hip OA models.

Siebenrock et al. reported a large animal model of experimentally induced FAI in sheep with deformity created via an intertrochanteric varus osteotomy[11]. This model is attractive but has some disadvantages, including high cost, limited availability compared with small animal models, a long timeline of experimental OA, and a difficult and invasive procedure. Additionally, it does not reproduce the natural etiology of cam-type FAI deformity. Recently, we used a novel approach by experimentally inducing an injury to the medial third of the proximal femoral epiphysis of an immature rabbit hip model, resulting in head-neck cam-type deformity[12]. The aim of our model was to create a head-neck deformity[13] that would result in intra-articular derangement and hip OA.

We hypothesized that the induced cam-type deformity in an immature rabbit hip model would lead to intra-articular derangement and progression of hip OA.

Materials and Methods

Animal Model

Thirty 6-week-old immature New Zealand White rabbits were subjected to right hip surgery. Of the 30 rabbits, 3 died during anesthesia prior to surgery and one experienced a postoperative local infection; the remaining 26 rabbits were included in the experiment. The contralateral left hips served as (nonsurgical) controls. This study received approval from the hospital and university Institutional Animal Care and Use Committee (#D16-00245). Only the person who performed the surgical procedures (C.P.-G.) knew which side was operated on, while all postoperative evaluations were performed in a blinded manner by coauthors (T.K. and K.K.). The study design is shown in Figure 1.

Surgical Procedure

All operations were performed as previously described[12]. Briefly, after the induction of general anesthesia, preoperative anteroposterior pelvic and frog-leg lateral radiographs were made with the rabbits in the supine position as a baseline for future assessment. After a 4-cm incision on the lateral right hip and muscle retraction, a T-shaped capsulotomy was performed. The femoral epiphysis was identified, and the femoral head was measured with a ruler. A $3 \times 2 \times 6$-mm defect in the epiphysis was created using a 1.6-mm drill bit, resulting in physeal injury. The hip joint was profusely irrigated. The capsule, fascia, and skin were sutured in separate layers. Postoperatively, the animals walked freely.

Radiographic Evaluation

At 4 and 16 weeks postsurgery, alpha angles were measured on anteroposterior pelvic and frog-leg lateral radiographs to assess head-neck deformity[12,14]. Depending on the hip joint radiograph feature, a semiquantitative, validated scoring system was used to evaluate the presence and severity of OA[15].

Bone Structure Evaluation

The hips were scanned using a vivaCT 40 micro-computed tomography (CT) scanner (70 kVp, 114 μA, 100-ms integration time, 30-μm resolution; SCANCO Medical) to analyze the femoral head deformity and subchondral bone structure. In accordance with a previous report[16], the region of interest was a 0.09-cm^2 circular area of subchondral trabecular bone in the 20 slices centered at a depth of 3.0 mm under the subchondral end plate of the femoral head. Bone morphometry values, including the bone volume/total volume ratio (BV/TV), trabecular thickness

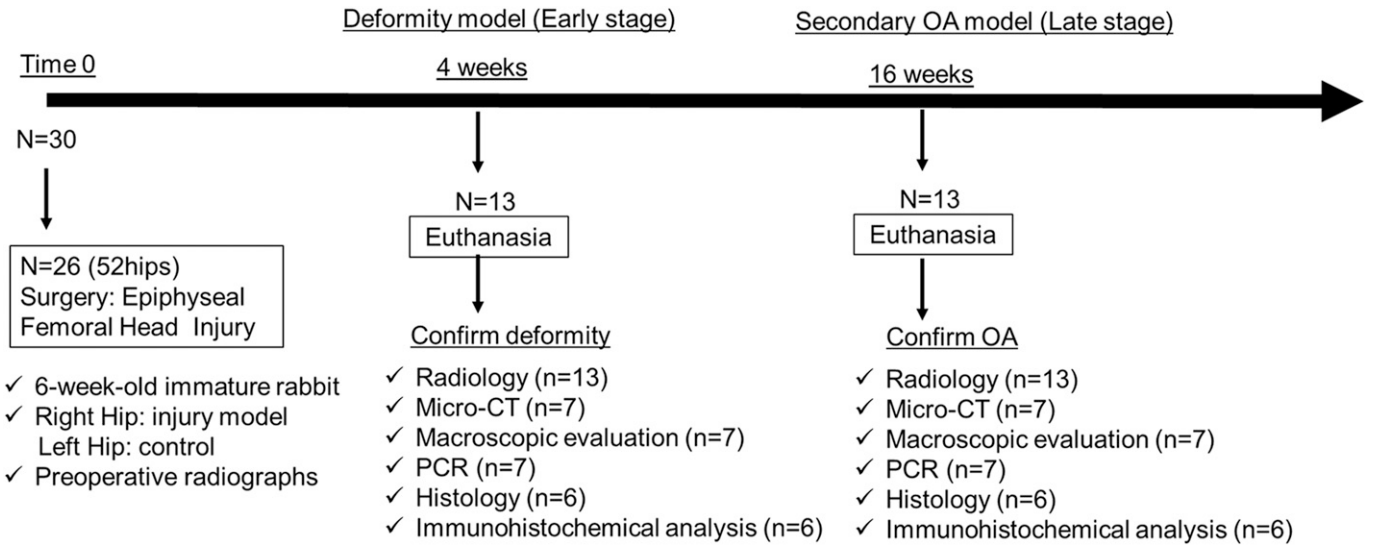

Fig. 1
Study design summary.

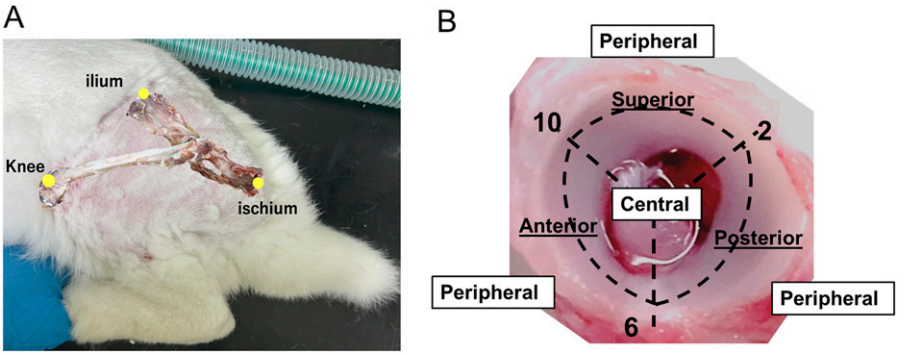

Fig. 2

Fig. 2-A Image showing the resting position of the femur and acetabulum. **Fig. 2-B** Section of a left acetabulum, with the assigned sectors being anterior at 6 to 10 o'clock, superior at 10 to 2 o'clock, and posterior at 2 to 6 o'clock).

(Tb.Th), trabecular spacing (Tb.Sp), and trabecular number (Tb.N), were measured using built-in software (SCANCO).

Macroscopic Evaluation

The rabbits were killed at the end of the ambulatory period (at 4 or 16 weeks), and both hip joints were dislocated for macroscopic evaluation and tissue processing (n = 7 per group). A schematic of the functional position of the femur and pelvis is shown in Figure 2-A. In accordance with a previous report[11], we defined 3 sectors of the acetabulum (anterior, superior, and posterior) for macroscopic and histological analysis, with 6 o'clock defined by the acetabular notch, and each section was divided into central and peripheral areas (Fig. 2-B). The chondral lesions were assessed using the Beck classification[1].

Gene Expression Analysis

Real-time polymerase chain reaction (RT-PCR) was used to assess the expression levels of genes of interest (n = 7 per group). Total RNA was extracted from cartilage tissue on the femoral head and acetabulum and was then reverse-transcribed into complementary DNA (cDNA) using a High-Capacity cDNA Reverse Transcription Kit (Applied Biosystems). RT-PCR amplification of the cDNA was performed in triplicates using SYBR Green reagent (Applied Biosystems). Relative gene expression was normalized against the housekeeping gene for glyceraldehyde 3-phosphate dehydrogenase (*GAPDH*) using the comparative cycle threshold method[17]. Relative gene expression was normalized to the mean value of control group samples for each gene. Primer sequences are listed in Table I.

Histological Analysis

Hips were fixed in 10% neutral buffered formalin for 24 to 48 hours, dehydrated, embedded in paraffin wax, and sectioned (5 μm). Deparaffinized coronal sections were stained with hematoxylin and eosin (HE) and safranin-O to evaluate cartilage and synovial degeneration. Articular cartilage damage and synovitis were quantified using the OA cartilage histopathology assessment system of the Osteoarthritis Research Society International (OARSI) (n = 6 per group)[18,19]. The acetabular area contacting the femoral head was defined as the weight-bearing area and the area outside (peripheral to) the femoral head, as the impingement area.

Immunofluorescence Analysis

Fluorescent immunostaining was performed in a previously described manner[20]. After deparaffinization, sections were permeabilized with sodium citrate buffer (10 mM sodium citrate, 0.05% Tween-20; pH 6.0) and blocked with 2.5% donkey serum for 2 hours at room temperature. Then, the sections were incubated with the primary antibodies against collagen type 2 (Col2) (1:10, Cat. # NB600-844; Novus Biologicals), collagen type 10 (Col10) (1:50, Cat. # 14-9771-80; Thermo Fisher), matrix metalloproteinase 13 (MMP13) (1:200, Cat. # NB1105919l; Fisher Scientific), and interleukin-1 beta (IL-1β) (1:20, Cat. # AA 118-268; antibodies-online) overnight at 4°C (n = 6 per group). After washing, the sections were incubated with the secondary antibody, Rhodamine Red-X AffiniPure Donkey Anti-Mouse IgG H&L (1:400, Cat. # 715-295-151; Jackson ImmunoResearch) for 2 hours. We used 4′,6′-diamidino-2-phenylindole (DAPI) (1:1,000; Vector Laboratories) for nuclei counterstaining for 5 minutes. The images were obtained in 5 randomly selected fields with a ZEISS LSM 880 Confocal Laser Scanning Microscope. The data for MMP13 and IL-1β are presented as the mean ratio of positive cells, which was

TABLE I Primer Sequences Used for Quantitative Real-Time-Polymerase Chain Reaction*

	Primer Sequence (5′-3′)	
Gene	Forward	Reverse
Col2	GCACCCATGGACATTGGAGG	AGCCCCGCACGGTCTTGCTT
Col10	GAAAACCAGGCTATGGAACC	GCTCCTGTAAGTCCCTGTTGTC
MMP13	TTCGAGTCATGCCACAAAT	TAAGCTTTGCCCTGAAACCT
GAPDH	CCCTCAATGACCACTTTGTG	GGTTTGAGGGCTCTTACTCCT

**Col2* = collagen type 2 gene, *COL10* = collagen type 10 gene, *MMP13* = matrix metalloproteinase 13 gene, *GAPDH* = glyceraldehyde 3-phosphate dehydrogenase gene.

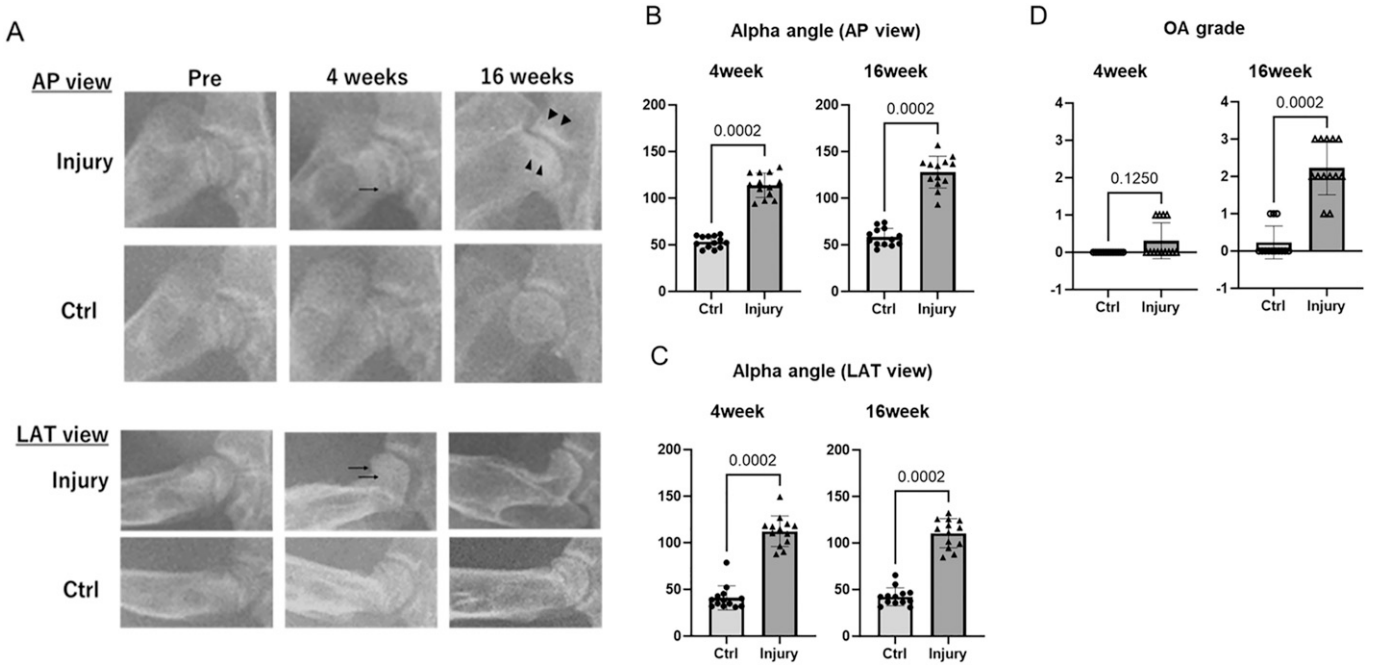

Fig. 3

Fig. 3-A Representative anteroposterior (AP) pelvic and frog-leg lateral (LAT) radiographs showing epiphyseal closure at the anteromedial femoral head (arrows) and OA progression including bone sclerosis, bone cystic lesion, and partial joint space narrowing (arrowheads). **Figs. 3-B and 3-C** Alpha angles on anteroposterior and frog-leg lateral radiographs at 4 and 16 weeks after injury. **Fig. 3-D** Radiographic OA grades at 4 and 16 weeks after injury. The graphs show the mean ± SD, with p values above the brackets. Ctrl = Control.

determined using the average cell count. The data for Col2 and Col10 are presented as the ratio relative to the pixel intensity in the control hips measured with ImageJ (National Institutes of Health).

Statistical Analysis

Statistical analyses were performed with GraphPad Prism, version 9.5.1 (GraphPad Software). Between-group comparisons were performed with the Wilcoxon signed-rank test for qualitative and quantitative variables. Significance was set at $p < 0.05$. Data are presented as the mean ± standard deviation.

Results

Radiographic Evaluation

Representative radiographic images are displayed in Figure 3. Radiographs at 4 weeks post-injury demonstrated epiphyseal closure at the anteromedial femoral head on both the anteroposterior and lateral radiographs (arrows, Fig. 3-A). The injured hips showed a varus tilt and an anterolateral protrusion of the femoral head, with higher alpha angles evident on both the anteroposterior (113.8° ± 13.0° versus 53.3° ± 6.3°, p = 0.0002) and lateral radiographs (112.3° ± 16.4° versus 41.0° ± 12.9°, p = 0.0002) compared with the controls at 4 weeks (Fig. 3-B) and at 16 weeks (127.9° ± 17.0° versus 58.3° ± 9.4°, p = 0.0002, and 110.5° ± 15.5° versus 42.3° ± 9.6°, p = 0.0002, on the anteroposterior and lateral views, respectively) (Fig. 3-C), confirming the asphericity of the injured femoral heads. Additionally, radiographs at 16 weeks clearly showed OA changes, including bone sclerosis, bone cystic lesions, and partial joint space narrowing (arrowheads, Fig. 3-A) in the injured hips, confirming OA progression compared with the control hips (OA grade: 2.17 ± 0.97 versus 0.16 ± 0.41, p = 0.0002) (Fig. 3-D).

Macroscopic Evaluation

At 4 weeks post-injury, minimal cartilage damage was observed, with acetabular cartilage fibrillation and partial thinning at the chondrolabral area (arrows, Fig. 4-A). No changes were observed on the femoral head. At 16 weeks, the disease had advanced, resulting in delamination, subchondral bone exposure, loss of cartilage integrity, and progression to OA, confirming a similar pattern of disease as seen in human hip OA due to FAI. On the femoral head, corresponding chondromalacia was present at the head-neck junction at 4 weeks post-injury (arrows, Fig. 4-B) and lesions progressed centrally to the perifoveal area at 16 weeks (arrowheads, Fig. 4-B). The injured hips exhibited a greater prevalence and severity of chondral lesions at 4 weeks (85.7 %, p = 0.015) and 16 weeks (100.0%, p = 0.002) post-injury compared with the control hips (0%). At 16 weeks, the injured hips demonstrated a significantly higher prevalence of macroscopic chondral lesions (Fig. 4-C) in the acetabular area compared with the control hips and a higher grade of peripheral cartilage damage compared with 4 weeks (p = 0.016; Fig. 4-D). Similarly, significant cartilage disease was observed on the femoral head at 16 weeks.

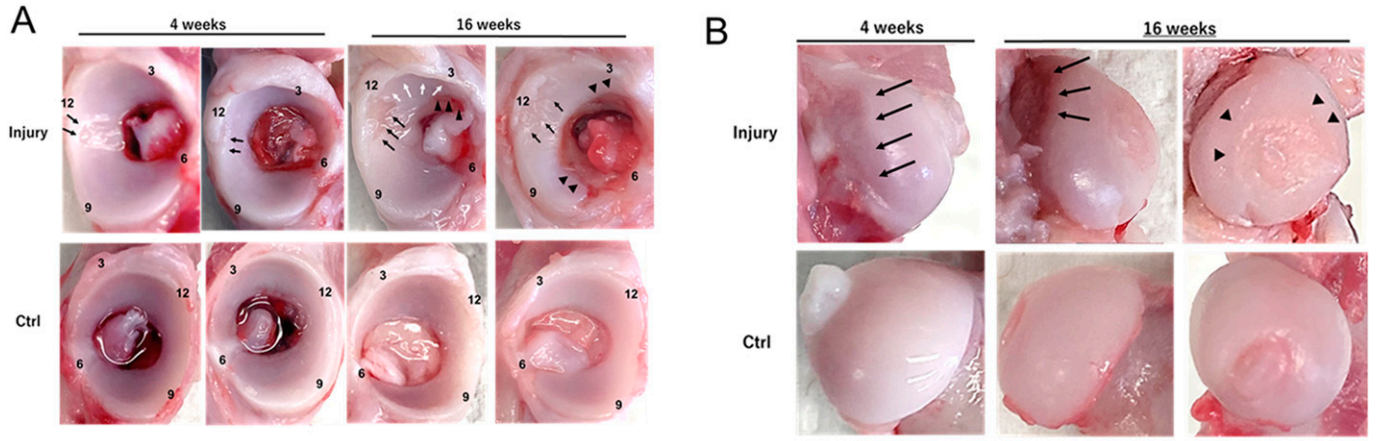

C

Prevalence of acetabular chondral lesions

	4 weeks	*16 weeks*	*P-value*
Peripheral			
Anterior	3/7	4/7	
Superior	6/7	7/7	
Posterior	1/7	3/7	
Total	**6/7**	**7/7**	**0.99**
Central			
Anterior	1/7	5/7	
Superior	1/7	5/7	
Posterior	0/7	2/7	
Total	**1/7**	**6/7**	**0.008**

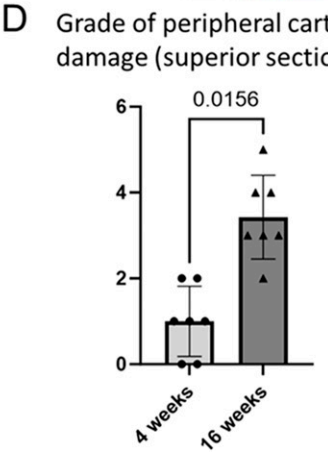

Fig. 4

Figs. 4-A and 4-B Representative macroscopic images of cartilage in the acetabulum (**Fig. 4-A**) and femoral head (**Fig. 4-B**). See the text ("Macroscopic Evaluation") for details of the findings. **Fig. 4-C** Prevalence of acetabular chondral lesions. **Fig. 4-D** Macroscopic OA grades in the peripheral superior area. The graph shows the mean ± SD, with the p value above the brackets. Ctrl = control.

Bone Structure Evaluation

No significant differences in any structural parameters were observed between the injured and control hips at 4 weeks. However, the femoral head BV/TV, femoral head Tb.Th, and acetabular BV/TV were significantly higher in the injured hips than in the control hips at 16 weeks (Fig. 5).

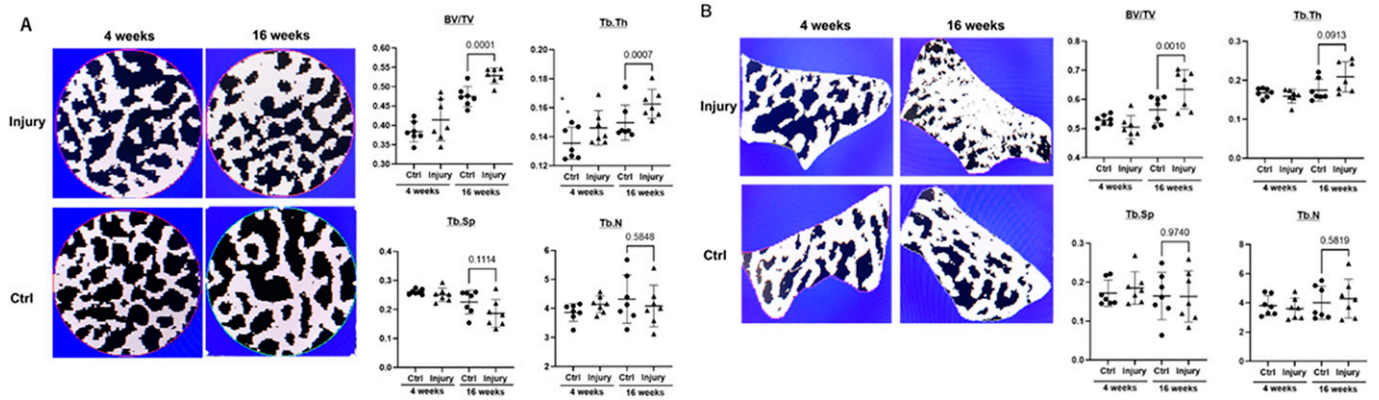

Fig. 5

Representative bone structure images of the femoral head (**Fig. 5-A**) and acetabulum (**Fig. 5-B**) and graphs comparing the BV/TV (bone volume/total volume), Tb.Th (trabecular thickness), Tb.Sp (trabecular spacing), and Tb.N (trabecular number) between the control (Ctrl) and injured hips at 4 and 16 weeks after injury. The graphs show the mean ± SD, with p values above the brackets.

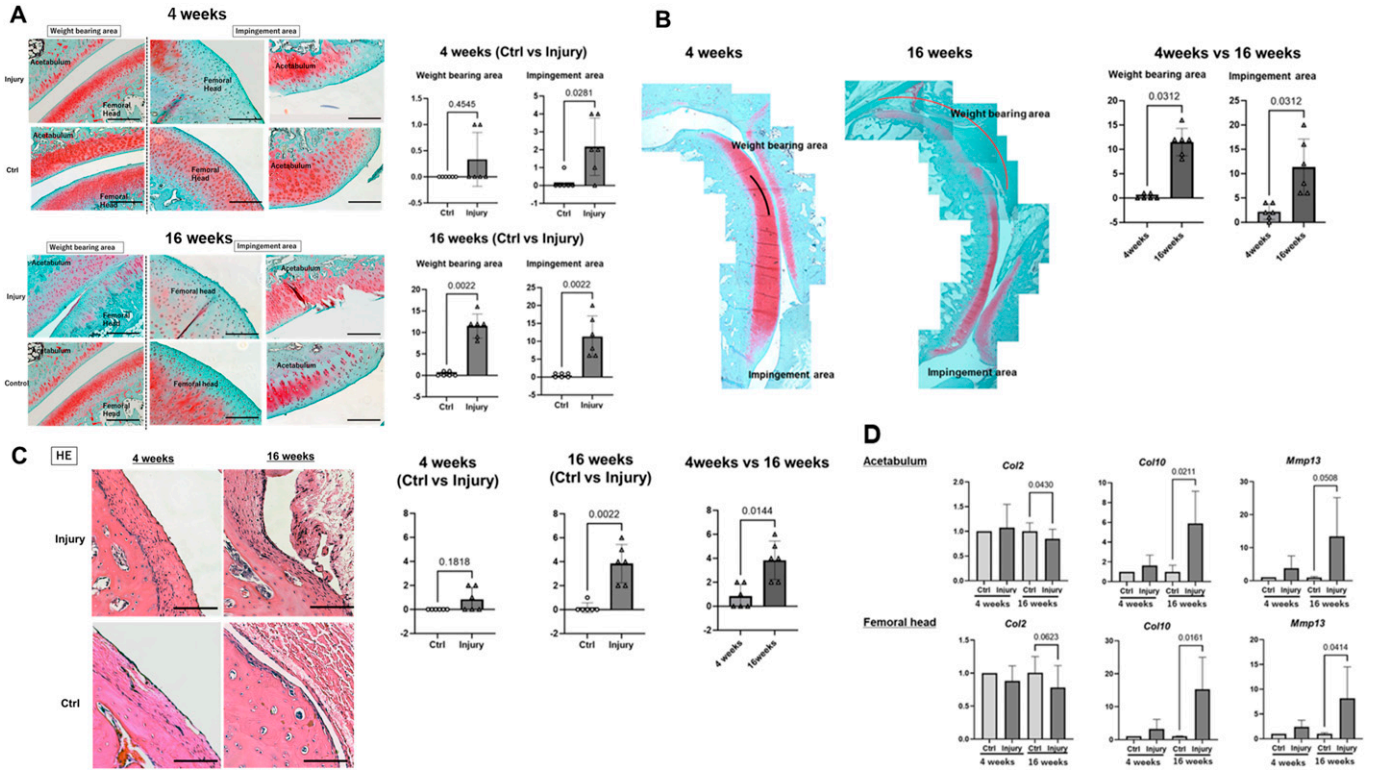

Fig. 6

Histological evaluation and gene expression analysis. **Fig. 6-A** Images of safranin-O-stained samples (bar = 1 mm) and graphs comparing the OARSI (Osteoarthritis Research Society International) scores in the weight-bearing and impingement areas between the control (Ctrl) and injured hips at 4 and 16 weeks after surgery. **Fig. 6-B** Low-magnification images of safranin-O-stained samples from the injured hips and graphs comparing the OARSI scores in the weight-bearing and impingement areas between the 4 and 16-week groups. **Fig. 6-C** Images of hematoxylin and eosin-stained samples of synovial tissue (bar = 1 mm) and graphs comparing the synovitis scores between the control and injured hips and between 4 and 16 weeks after surgery. **Fig. 6-D** Graphs comparing the relative expression of Col2 (collagen type 2), Col10 (collagen type 10), and MMP13 (matrix metalloproteinase 13) in cartilage samples between the control and injured hips.

Histological Analysis and Gene Expression Analysis

Hip cartilage samples at 4 weeks post-injury showed higher OARSI grades in the impingement head-neck region compared with the controls (2.18 ± 1.68 versus 0.17 ± 0.41, p = 0.028; Fig. 6-A), but no significant difference in the acetabular weight-bearing area (0.33 ± 0.52 versus 0.0 ± 0.0, p = 0.455; Fig. 6-A). However, at 16 weeks, cartilage samples from both the femoral impingement and acetabular zones had significantly higher OARSI grades in the injured group compared with the controls (p = 0.002 for both zones; Fig. 6-A), confirming the progression of OA, with an increased OARSI grade compared with 4 weeks post-injury (p = 0.031 for both zones; Fig. 6-B).

Synovitis was not observed in the control hips. In the injured hips, synovitis was minimal at 4 weeks post-injury (synovitis score, 0.83 ± 0.98) but progressed significantly at 16 weeks (synovitis score, 3.83 ± 1.60, p = 0.014) for 4 versus 16 weeks; Fig. 6-C). RT-PCR confirmed progression to OA as shown by increased expression of catabolic markers (*Col10* and *MMP13*) and decreased expression of *Col2* in the cartilage of the injured hips at 16 weeks (Fig. 6-D). Immunofluorescence cartilage staining at 16 weeks showed that the injured group had significantly increased Col10 expression (1.93 ± 0.18 versus 1.00 ± 0.09, p < 0.0001) and MMP13 expression (0.58 ± 0.06 versus 0.22 ± 0.05, p < 0.0001) and decreased Col2 expression (0.50 ± 0.04 versus 1.00 ± 0.10, p < 0.0001) compared with the controls (Figs. 7-A and 7-B). Immunofluorescence staining of the synovium at 16 weeks post-injury demonstrated significant increases in MMP13 expression (0.17 ± 0.006 versus 0.037 ± 0.005, p = 0.031) and IL-1β expression (0.20 ± 0.019 versus 0.033 ± 0.015, p = 0.031) compared with the controls (Figs. 8-A and 8-B).

Discussion

The experimentally induced hip deformity in our proposed model resulted in documented hip OA. To our knowledge, this is the first reported small animal model of induced head-neck deformity resulting in hip OA progression. The deformity was confirmed radiographically, macroscopically, histologically, with PCR, and with micro-CT. This model will be clinically relevant, as it can be used to study mechanisms of hip OA secondary to head-neck deformity and test future interventional therapies.

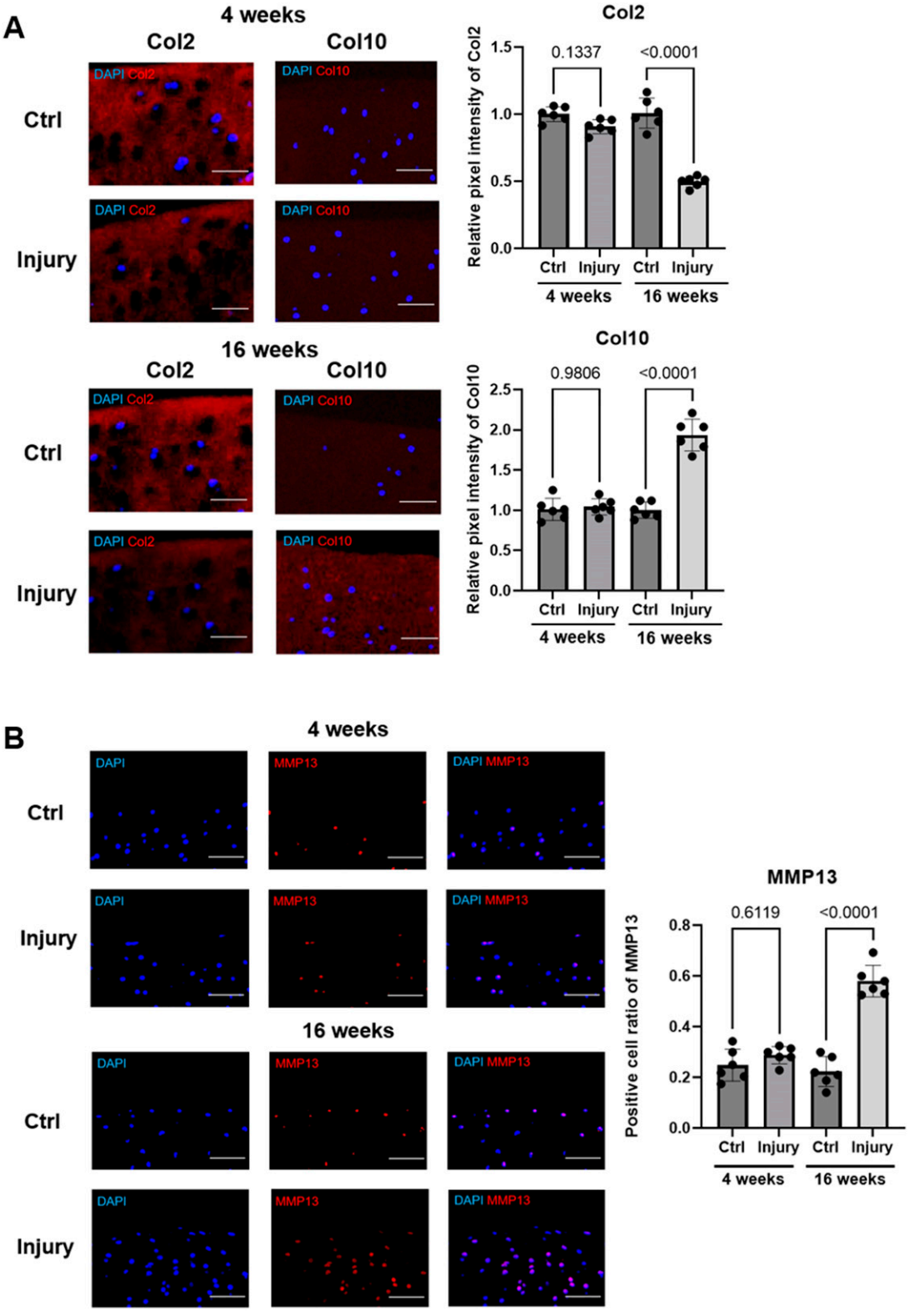

Fig. 7

Immunofluorescence staining of cartilage samples (bar = 50 μm), with graphs showing their relative pixel intensity of Col2 (collagen type 2) and Col10 (collagen type 10) (**Fig. 7-A**) and the proportion of cells positive for MMP13 (matrix metalloproteinase 13) (**Fig. 7-B**) in the control (Ctrl) hips and injured hips at 4 and 16 weeks after surgery.

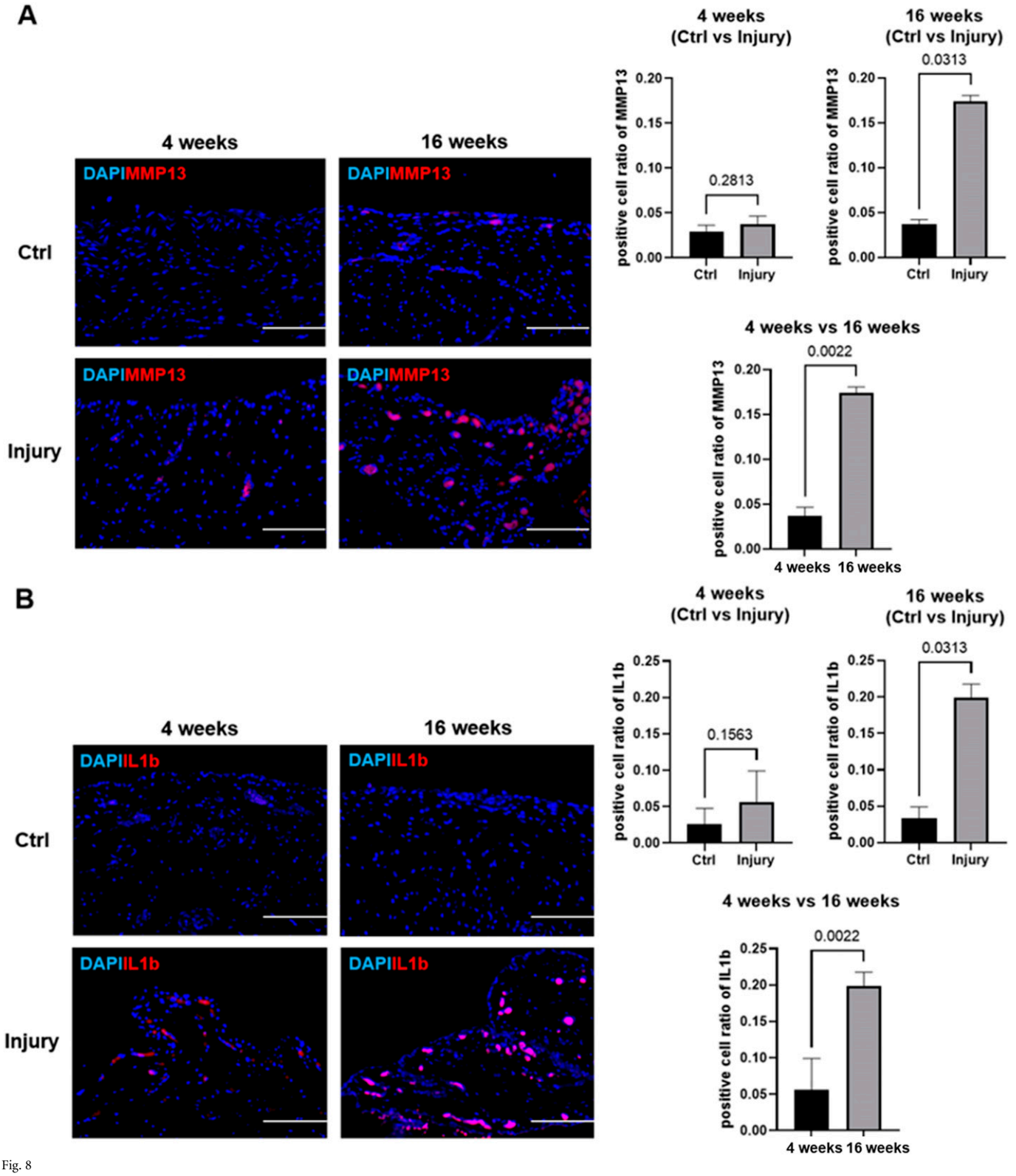

Fig. 8

Immunofluorescence staining of synovial samples (bar = 100 μm), and graphs showing the proportion of cells positive for MMP13 (matrix metalloproteinase 13) (**Fig. 8-A**) and IL-1β (interleukin-1 beta) (**Fig. 8-B**) in the control (Ctrl) and injured hips at 4 and 16 weeks after surgery.

Studies suggest that a cam morphology can develop during adolescence through alterations in the capital femoral epiphysis in response to participation in vigorous sports activity[21,22]. Uneven pressures applied during rigorous physical activities by young athletes can lead to asymmetric epiphyseal closure and cause angular deformities of the femoral head-neck junction that result in cam deformity[23,24]. During development, the normal pressure of the femoral head in the acetabulum maintains a balance of acetabular triradiate cartilage growth. The shape of the proximal femur depends primarily on the contributions of the proximal femoral growth plates. Alterations in any of these growth plates result in proximal femoral deformities[25]. On the basis of these findings, we experimentally created an injury to the medial third of the proximal femoral epiphysis in immature rabbit hips to induce a cam-type deformity. Only 1 large animal (sheep) model in which hip impingement was induced by extra-articular varus osteotomy has been reported[11,26]. This model successfully recreated intra-articular damage and hip OA progression[11,26]. Our model has the advantage of inducing a head-neck deformity with a relatively low-cost, minimally invasive approach that reproduces a more natural model of deformity.

Our model exhibited varus tilt of the femoral head and asphericity of the femoral head-neck junction on radiographs at 4 weeks post-injury and subsequent OA progression compared with controls. Micro-CT analysis showed higher subchondral BV/TV and femoral head Tb.Th, confirming OA changes in bone structure. Macroscopically, the acetabular cartilage degeneration was already evident at the superior peripheral area at 4 weeks, and its severity progressed through 16 weeks, which is similar to the cartilage-damage pattern of human cam-type FAI[27]. The location of these lesions differs from that in the previously reported large (sheep) animal model[11]. In that model, chondrolabral lesions were seen in the posterosuperior area of the acetabulum, which differs from the cartilage damage pattern of human cam-type FAI[27]. This difference between our proposed rabbit model and the sheep model could be explained by the deeper flexion reached in the gait of rabbits and humans compared with sheep. Another reason could be that our model resulted in a different pattern of head-neck deformity compared with that created by an extra-articular varus osteotomy, resulting in a different area of collision and damage.

Progression of OA was confirmed histologically and with RT-PCR. OA changes initiated at the peripheral acetabulum and spread centrally over 16 weeks. The severity of OA and synovitis increased from 4 to 16 weeks post-injury. Cartilage samples from the acetabulum and femoral head demonstrated decreased *Col2* expression and increased *Col10* and *MMP13* expression from 4 to 16 weeks post-injury, confirming the progression of cartilage degeneration, catabolism, and chondrocyte hypertrophy[28]. In the future, transcriptome analysis may be used to identify the major molecular pathways of this model that contribute to the progression of hip OA and determine if these pathways are consistent with the well-known pathways reported in previous animal and human OA studies[7,29]. In addition, this model provides an opportunity to examine the impact of inhibitors and activators of the relevant pathways on slowing disease progression.

There are some limitations in the proposed animal model. Gait and anatomical differences between rabbits and humans, as well as the innate dissimilarity of their hip joints, limit translation of findings based on this model to human FAI. It should be noted that we initially tried a mouse model for physeal injury, but the small joint size led to inconsistent injury patterns and no FAI-like features.

Another limitation is that this model does not allow for specific gene knockouts, limiting the understanding of the functional effects of specific genes in hip OA progression. Also, our use of an immature animal model to induce an adult hip disease might be considered a weakness. However, we believe that the young age in our model is a strength since the etiology of cam-FAI occurs in humans during skeletal development when the physis is still open. An additional limitation is that we did not perform sham surgery on the contralateral hip. This can lead to questions regarding how much of the OA was secondary to the trauma from the surgery rather than to the physeal injury. However, our approach is minimally invasive, with the procedure performed through a small capsulotomy that we do not believe would generate enough trauma to generate an inflammatory response leading to OA. Lastly, we did not assess range of motion in our animals. Normal and pathological ranges of motion of rabbits have not been published in the veterinary literature, to our knowledge.

We have validated our deformity using statistical shape modeling, which showed it to be located in the anterosuperior aspect of the head-neck junction[30]. We are currently investigating cartilage stresses using finite element analysis to better understand the impingement zones in our model and subsequent changes in cartilage stresses during different ranges of motion and ambulation and to evaluate the mechanical properties of cartilage using nanoindentation during the progression of FAI OA in this model. We believe that these critical mechanisms should be further investigated and could uniquely impact future hip OA treatment.

Conclusion

This study provides a novel rabbit model for inducing femoral head-neck deformity and demonstrated secondary OA changes, confirmed radiographically, histologically, and via gross inspection. We believe that this model could serve as a benchmark for future understanding of the biological changes in mechanically induced hip arthritis and for testing future interventional therapies. ■

Tomoyuki Kamenaga, MD, PhD[1,2]
Kenichi Kikuchi, MD, PhD[1]
Regis J. O'Keefe, MD, PhD[1]
John C. Clohisy, MD[1]
Cecilia Pascual-Garrido, MD, PhD[1]

[1]Department of Orthopaedic Surgery, Washington University in St. Louis School of Medicine, St. Louis, Missouri

[2]Department of Orthopaedic Surgery, Kobe University Graduate School of Medicine, Kobe, Japan

Email for corresponding author: cpascualgarrido@wustl.edu

References

1. Beck M, Kalhor M, Leunig M, Ganz R. Hip morphology influences the pattern of damage to the acetabular cartilage: femoroacetabular impingement as a cause of early osteoarthritis of the hip. J Bone Joint Surg Br. 2005 Jul;87(7):1012-8.

2. Ganz R, Parvizi J, Beck M, Leunig M, Nötzli H, Siebenrock KA. Femoroacetabular impingement: a cause for osteoarthritis of the hip. Clin Orthop Relat Res. 2003 Dec;(417):112-20.

3. Haneda M, Rai MF, Cai L, Brophy RH, O'Keefe RJ, Clohisy JC, Pascual-Garrido C. Distinct Pattern of Inflammation of Articular Cartilage and the Synovium in Early and Late Hip Femoroacetabular Impingement. Am J Sports Med. 2020 Aug;48(10):2481-8.

4. Haneda M, Rai MF, O'Keefe RJ, Brophy RH, Clohisy JC, Pascual-Garrido C. Inflammatory Response of Articular Cartilage to Femoroacetabular Impingement in the Hip. Am J Sports Med. 2020 Jun;48(7):1647-56.

5. Hashimoto S, Rai MF, Gill CS, Zhang Z, Sandell LJ, Clohisy JC. Molecular characterization of articular cartilage from young adults with femoroacetabular impingement. J Bone Joint Surg Am. 2013 Aug 21;95(16):1457-64.

6. Chinzei N, Hashimoto S, Fujishiro T, Hayashi S, Kanzaki N, Uchida S, Kuroda R, Kurosaka M. Inflammation and Degeneration in Cartilage Samples from Patients with Femoroacetabular Impingement. J Bone Joint Surg Am. 2016 Jan 20;98(2):135-41.

7. Pascual-Garrido C, Kamenaga T, Brophy RH, Shen J, O'Keefe RJ, Clohisy JC. Otto Aufranc Award: Identification of Key Molecular Players in the Progression of Hip Osteoarthritis Through Transcriptomes and Epigenetics. J Arthroplasty. 2022 Jul;37(7S):S391-9.

8. Hall M, van der Esch M, Hinman RS, Peat G, de Zwart A, Quicke JG, Runhaar J, Knoop J, van der Leeden M, de Rooij M, Meulenbelt I, Vliet Vlieland T, Lems WF, Holden MA, Foster NE, Bennell KL. How does hip osteoarthritis differ from knee osteoarthritis? Osteoarthritis Cartilage. 2022 Jan;30(1):32-41.

9. Rushton MD, Reynard LN, Barter MJ, Refaie R, Rankin KS, Young DA, Loughlin J. Characterization of the cartilage DNA methylome in knee and hip osteoarthritis. Arthritis Rheumatol. 2014 Sep;66(9):2450-60.

10. den Hollander W, Ramos YF, Bos SD, Bomer N, van der Breggen R, Lakenberg N, de Dijcker WJ, Duijnisveld BJ, Slagboom PE, Nelissen RG, Meulenbelt I. Knee and hip articular cartilage have distinct epigenomic landscapes: implications for future cartilage regeneration approaches. Ann Rheum Dis. 2014 Dec;73(12):2208-12.

11. Siebenrock KA, Fiechter R, Tannast M, Mamisch TC, von Rechenberg B. Experimentally induced cam impingement in the sheep hip. J Orthop Res. 2013 Apr;31(4):580-7.

12. Kamenaga T, Haneda M, Brophy RH, O'Keefe RJ, Clohisy JC, Pascual-Garrido C. A Novel Model of Hip Femoroacetabular Impingement in Immature Rabbits Reproduces the Distinctive Head-Neck Cam Deformity. Am J Sports Med. 2022 Jun;50(7):1919-27.

13. Rowe SM, Lee JJ, Chung JY, Moon ES, Song EK, Seo HY. Deformity of the femoral head following vascular infarct in piglets. Acta Orthop. 2006 Feb;77(1):33-8.

14. Nötzli HP, Wyss TF, Stoecklin CH, Schmid MR, Treiber K, Hodler J. The contour of the femoral head-neck junction as a predictor for the risk of anterior impingement. J Bone Joint Surg Br. 2002 May;84(4):556-60.

15. Arzi B, Wisner ER, Huey DJ, Kass PH, Hu J, Athanasiou KA. A proposed model of naturally occurring osteoarthritis in the domestic rabbit. Lab Anim (NY). 2011 Dec 19;41(1):20-5.

16. Chiba K, Ito M, Osaki M, Uetani M, Shindo H. In vivo structural analysis of subchondral trabecular bone in osteoarthritis of the hip using multi-detector row CT. Osteoarthritis Cartilage. 2011 Feb;19(2):180-5.

17. Livak KJ, Schmittgen TD. Analysis of relative gene expression data using real-time quantitative PCR and the 2(-Delta Delta C(T)) Method. Methods. 2001 Dec;25(4):402-8.

18. Laverty S, Girard CA, Williams JM, Hunziker EB, Pritzker KP. The OARSI histopathology initiative - recommendations for histological assessments of osteoarthritis in the rabbit. Osteoarthritis Cartilage. 2010 Oct;18(Suppl 3):S53-65.

19. Krenn V, Morawietz L, Burmester GR, Kinne RW, Mueller-Ladner U, Muller B, Haupl T. Synovitis score: discrimination between chronic low-grade and high-grade synovitis. Histopathology. 2006 Oct;49(4):358-64.

20. Kamenaga T, Shen J, Wu M, Brophy RH, Clohisy JC, O'Keefe RJ, Pascual-Garrido C. Epigenetic dysregulation of articular cartilage during progression of hip femoroacetabular impingement disease. J Orthop Res. 2023 Aug;41(8):1678-86.

21. Siebenrock KA, Wahab KH, Werlen S, Kalhor M, Leunig M, Ganz R. Abnormal extension of the femoral head epiphysis as a cause of cam impingement. Clin Orthop Relat Res. 2004 Jan;(418):54-60.

22. Morris WZ, Li RT, Liu RW, Salata MJ, Voos JE. Origin of Cam Morphology in Femoroacetabular Impingement. Am J Sports Med. 2018 Feb;46(2):478-86.

23. Cho YJ, Jung GY, Kim EJ, Chun YS, Rhyu KH. Asymmetric epiphyseal closure of the femoral head as a potential cause of the primary cam lesion: a case report. Skeletal Radiol. 2016 Sep;45(9):1299-302.

24. Agricola R, Heijboer MP, Ginai AZ, Roels P, Zadpoor AA, Verhaar JA, Weinans H, Waarsing JH. A cam deformity is gradually acquired during skeletal maturation in adolescent and young male soccer players: a prospective study with minimum 2-year follow-up. Am J Sports Med. 2014 Apr;42(4):798-806.

25. Siffert RS. Patterns of deformity of the developing hip. Clin Orthop Relat Res. 1981 Oct;(160):14-29.

26. Zurmühle CA, Schmaranzer F, Nuss K, Wolfer N, Ryan MK, Zheng G, von Rechenberg B, Tannast M. Proof of concept: hip joint damage occurs at the zone of femoroacetabular impingement (FAI) in an experimental FAI sheep model. Osteoarthritis Cartilage. 2019 Jul;27(7):1075-83.

27. Pascual-Garrido C, Li DJ, Grammatopoulos G, Yanik EL, Clohisy JC; ANCHOR Group. The Pattern of Acetabular Cartilage Wear Is Hip Morphology-dependent and Patient Demographic-dependent. Clin Orthop Relat Res. 2019 May;477(5):1021-33.

28. He Y, Siebuhr AS, Brandt-Hansen NU, Wang J, Su D, Zheng Q, Simonsen O, Petersen KK, Arendt-Nielsen L, Eskehave T, Hoeck HC, Karsdal MA, Bay-Jensen AC. Type X collagen levels are elevated in serum from human osteoarthritis patients and associated with biomarkers of cartilage degradation and inflammation. BMC Musculoskelet Disord. 2014 Sep 22;15:309.

29. Kuhns BD, Reuter JM, Hansen VL, Soles GL, Jonason JH, Ackert-Bicknell CL, Wu CL, Giordano BD. Whole-genome RNA sequencing identifies distinct transcriptomic profiles in impingement cartilage between patients with femoroacetabular impingement and hip osteoarthritis. J Orthop Res. 2023 Jul;41(7):1517-30.

30. Ince DC, Kamenaga T, Kikuchi K, Clohisy JC, O'Keefe RJ, Yuh C, Wimmer MA, Mell SP, Pascual-Garrido C. Statistical Shape Modeling of an Experimental Induced FAI Cam Deformity in a Rabbit Model. A Platform to Study Mechanism of Hip Disease. Am J Sports Med (in press).